Supporting Information

Rational Molecular Design of Phenanthroimidazole-Based Fluorescent Materials towards High-Efficiency Non-Doped Deep Blue OLEDs

Chunya Du,[a] Tong Lu,[a] Zhuang Cheng,[a] Yulei Chang,[b] Hui Liu,[c] Jun Wang,[d] Liang Wan,[a] Ying Lv[b] and Ping Lu*,[a]

[a] State Key Laboratory of Supramolecular Structure and Materials, Department of Chemistry, Jilin University, Changchun 130012, China.

[b] State Key Laboratory of Luminescence and Applications, Changchun Institute of Optics, Fine Mechanics and Physics, Chinese Academy of Sciences, Changchun 130033, China

[c] College of Optoelectronic Engineering, Chengdu University of Information Technology, Chengdu 610225, China;

[d] National & Local Joint Engineering Laboratory for Synthesis Technology of High Performance Polymer, Key Laboratory of High Performance Plastics, Ministry of Education, College of Chemistry, Jilin University, Qianjin Street 2699, Changchun, 130012, P. R. China

*Corresponding author: lup@jlu.edu.cn

Table of Contents

1. Experimental Section

General Methods

The materials employed in this paper and all the solvents and reagents used for synthesis and measurements were purchased from commercial suppliers without further purification unless otherwise stated. The mass spectra were tested using MALDI-TOF-MS method with AXIMA-CFRTM plus instruments. The NMR data were recorded on a Bruker AVANCE 500 spectrometer at 500 MHz, and the tests used tetramethylsilane (TMS) as internal standard and DMSO-D_6 as solvents. Elemental analysis was finished on a Flash EA 1112, CHNS-O elemental analysis instrument. Single crystal X-ray diffraction intensity data were collected at room temperature on a Rigaku R-AXIS RAPID diffractometer using the ω-scan mode with graphite-monochromated Mo Kα radiation (0.71073 Å). The crystal structures were solved with direct methods and refined with a full-matrix least-squares technique using the SHELXS programs. All angles and distances in crystals were measured using Mecury 1.4.1 Software. Thermal gravimetric analysis (TGA) data were collected from a Perkin-Elmerthermal analysis system under nitrogen protection (30 to 800 °C), the heating rate is 10 K min^{-1}. Differential scanning calorimetry (DSC) was measured on a NETZSCH (DSC-204) unit from 30 to 360 °C at a heating rate of 10 K min^{-1} with nitrogen atmosphere. The electrochemical properties were performed via cyclic voltammetry (CV) measurements. The tests used a standard one-compartment, three-electrode electrochemical cell given by a BAS 100 B/W electrochemical analyzer, where tetrabutylammoniumhexafluorophosphate ($TBAPF_6$) in anhydrous dimethyl formamide (DMF) or anhydrous dichloromethane with the concentration of 0.1 M were used as the electrolytes for negative or positive scans to calculate the oxidation and reduction potentials of the materials. The resulting HOMO/LUMO values are calculated according to the equation: (unit: eV)

$$E_{\mathrm{HOMO}} = -(E_{\mathrm{ox}} \text{ vs. } \mathrm{Fc/Fc^+} + 4.8) \qquad \textbf{Equation S1}$$

$$E_{\mathrm{LUMO}} = -(E_{\mathrm{red}} \text{ vs. } \mathrm{Fc/Fc^+} + 4.8) \qquad \textbf{Equation S2}$$

Photophysical Measurement

UV-vis, fluorescence spectra and PLQY (Φ_F) were recorded on a Shimadzu UV-3100 spectrophotometer using 1 cm path length quartz cells. Photoluminescence tests were measured by FLS920 spectrophotometer with steady and transient modes. PL spectra are obtained with a Xenon light source and further fluorescence lifetimes were measured using a 280 nm picosecond pulsed light emitting diode excitation source. The Φ_F of different solutions were determined by using quinine sulfate as a reference (Φ_F = 0.546) and were calculated by using the following formula:

$$Q_x = Q_r\left(\frac{A_r(\lambda_r)}{A_x(\lambda_x)}\right)\left(\frac{I(\lambda_r)}{I(\lambda_x)}\right)\left(\frac{n_x^2}{n_r^2}\right)\left(\frac{D_x}{D_r}\right)$$

Equation S3

Where Q is the PLQY, A is the value of absorbance, I is the intensity of excitation source, n is the refractive index of solvent, D is the area of emission spectra, λ is the corresponding wavelength. The subscript r stands for the reference while x stands for test subject. The excitation wavelength was 330 nm for PPI-2-DMF, PPI-2-DPF and PPI-3-SBF.

The k_r and k_{nr} mentioned are calculated according to the equations:

$$k_r = \frac{\Phi}{\tau}$$

Equation S4

$$k_{nr} = \frac{1 - \Phi}{\tau}$$

Equation S5

where ϕ is the PLQY measured by a integrating sphere attachment of FLS920 spectrophotometer, τ is the corresponding lifetimes of the emitters.

To determine emitting dipole orientation of an emitting film, angle-resolved and polarization-resolved PL measurements were performed. The sample consisted of a silica substrate with the 30-nm thick neat film. The sample was attached to a half quartz cylinder prism by index matching liquid. The excitation of the samples was performed with the 325-nm line of the continuous-wave He: Cd laser with a fixed excitation angle

of 45°. The emission angle was changed by use of an automatic rotation stage. The spectra were resolved by utilization of a p-polarizing filter and measured by a fiber optical spectrometer. The angle-dependent p-polarized emission intensity at the peak wavelength of the PL spectrum of the emitting layer was detected. The emitting dipole orientation ($\Theta_{//}$) was then determined by least-square fitting of the measured angle dependent p-polarized emission intensity with calculated results.

Lippert-Mataga calculation

$$hc(\nu_a - \nu_f) = hc(\nu_a^0 - \nu_f^0) - \frac{2(\mu_e - \mu_g)^2}{a^3} f(\varepsilon, n)$$

Equation S6

f is the orientational polarizability of the solvent, corresponds to the Stokes shifts when f is zero, μ_e is the excited state dipole moment, μ_g is the ground-state dipole moment; a is the solvent cavity (Onsager) radius, derived from the Avogadro number (N), molecular weight (M), and density (d = 1.0 g/cm^3); ε and n are the solvent dielectric and the solvent refractive index, respectively; a and f (ε, n) can be calculated respectively as follows:

$$f(\varepsilon,n) = \frac{\varepsilon - 1}{2\varepsilon + 1} - \frac{n^2 - 1}{2n^2 + 1}$$

Equation S7

$$a = (3M/4N\pi l)^{1/3}$$

Equation S8

The detailed data are listed in Table S2~S3. The stokes shift $(\nu_a - \nu_f)$ of PPI-2-DMF, PPI-2-DPF and PPI-3-SBF are in linear relationship with the solvent polarity f as presented in Fig. 3c.

Device Fabrication

The purchased ITO glass was used as the substrate after carefully cleaned with isopropyl alcohol, acetone, toluene and deionized water, then go through drying

procedure at 120 °C in an oven and UV-zone treatment. The sheet resistance of the ITO glass is 20 Ω square^{-1}. The prepared ITO glasses were transfer to the deposition system in the glove box with vacuum condition. All the organic layers were deposited at a rate of 1.0 Å s^{-1} , the deposition rate for cathode LiF and the capping Al metal layer were 0.1 and 4.0 Å s^{-1}. The electroluminescent (EL) characteristics were measured under ambient condition at room temperature, using a Keithley 2400 programmable electrometer and CS-200 chromameter. EL spectra are collected on a PR-650 Spectroscan spectrometer.

$$EQE = (\gamma \times \eta_r \times \eta_{PL}) \times \eta_{out}$$ **Equation S9**

where η_{PL} is the PLQY of the emitters in corresponding solid state; γ is the charge recombination factor of the devices which is approximately equal to 1 if the device is best optimized considering that the injected holes and electrons are balanced and completely recombined to form excitons; η_{out} is the light out-coupling efficiency which is estimated as 20-30 % according to the emitting region; η_r is the efficiency of radiative exciton production.

The transient EL decay was tested by an Agilent 8114A pulse generator (100 V/2 A) to generate rectangular pulse voltages. The pulse repetition rate was 500 Hz with the width of 500 μs. The EL signal was detected using a lens coupled with the optical fiber connected to a Hamamatsu photomultiplier (H10721-20) with time resolution of 0.57 ns. The photomultiplier was connected to one of the channels of a digital oscilloscope (Tektronix DPO5204B, sampling rate: 10 GS s-1; resolution: 100 μV) with 50 Ω input resistance.

Theoretical Calculation Method

The ground-state (S_0) geometries were optimized at the B3LYP/6-31G(d, p) level, and the HOMO/LUMO distributions are calculated on the basis of optimized S_0 state. The higher energy levels of both singlet and triplet states were calculated using TD-B3LYP/6-31G(d, p) method on the basis of the optimized configuration of S_1. Natural transition orbitals (NTOs) involving both singlet and triplet states were evaluated to

investigate the properties of excited state.

2 Synthesis and Characterization

2. 1. 2-(4-(9,9-dimethyl-9H-fluoren-2-yl)phenyl)-1-phenyl-1H-phenanthro[9,10-d]imidazole (PPI-2-DMF)

A mixture of 2-bromo-9,9-dimethylfluorene (1.64 g, 6 mmol), PPIB (2.47 g, 5 mmol), $Pd(PPh_3)_4$ (0.17 g, 0.15 mmol), K_2CO_3 (5.52 g, 40 mmol), 20 mL distilled water, 40 mL toluene and were added to a 100 mL round flask and refluxed at 90 °C for 24 hours under nitrogen protection. Then the mixture was poured into water and extracted with dichloromethane for three times. After being collected and concentrated, the organic phase was then purified by column chromatography using petroleum ether/dichloromethane as eluent to finally afford white solid. ^{1}H NMR (500 MHz, DMSO-D_6) δ (ppm): 8.95 (d, J = 8.2 Hz, 1H), 8.90 (d, J = 8.4 Hz, 1H), 8.74 (d, J = 6.9 Hz, 1H), 7.92 (dd, J = 11.7, 4.6 Hz, 2H), 7.87 (d, J = 6.6 Hz, 1H), 7.84 - 7.67 (m, 12H), 7.58 (dd, J = 8.6, 4.4 Hz, 2H), 7.39 - 7.32 (m, 3H), 7.10 (d, J = 8.0 Hz, 1H), 1.50 (s, 6H)

MS (MALDI-TOF), m/z: calcd for $C_{42}H_{30}N_2$, 562.25; Found, 562.75 [M+]. Anal. Calcd for $C_{42}H_{30}N_2$, C, 89.65; H, 5.37; N, 4.98 %; Found, C, 89.67, H, 5.39, N, 4.94%.

2. 2. 2-(4-(9,9-diphenyl-9H-fluoren-2-yl)phenyl)-1-phenyl-1H-phenanthro[9,10-d]imidazole (PPI-2-DPF)

A mixture of 2-bromo-9,9-diphenylfluorene (2.38 g, 6 mmol),PPIB (2.47 g, 5 mmol), $Pd(PPh_3)_4$ (0.17 g, 0.15 mmol), K_2CO_3 (5.52 g, 40 mmol), 20 mL distilled water, 40 mL toluene and were added to a 100 mL round flask and refluxed at 90 °C for 24 hours under nitrogen protection. Then the mixture was poured into water and extracted with dichloromethane for three times. After being collected and concentrated, the organic phase was then purified by column chromatography using petroleum ether/dichloromethane as eluent to finally afford white solid. ^{1}H NMR (500 MHz, DMSO-D_6) δ (ppm): 8.94 (d, J = 8.3 Hz, 1H), 8.88 (s, 1H), 8.71 (d, J = 8.0 Hz, 1H),

8.04 (d, J = 8.0 Hz, 2H), 7.99 (s, 1H), 7.82 - 7.68 (m, 8H), 7.66 (s, 3H), 7.56 (d, J = 7.1 Hz, 2H), 7.44 (t, J = 8.1 Hz, 2H), 7.37 - 7.33 (m, 2H), 7.26 (dd, J = 17.1, 7.4 Hz, 5H), 7.19 (d, J = 7.0 Hz, 4H), 7.08 (d, J = 7.7 Hz, 2H). MS (MALDI-TOF), m/z: calcd for $C_{52}H_{34}N_2$, 686.72; Found, 686.68 [M+]. Anal. Calcd for $C_{52}H_{34}N_2$, C,90.93; H, 4.99; N, 4.08 %; Found, C, 90.91, H, 4.99, N, 4.10%.

2. 3. 2-(4-(9,9'-spirobi[fluoren]-3-yl)phenyl)-1-phenyl-1H-phenanthro[9,10-d]imidazole (PPI-3-SBF)

A mixture of 3-bromo-9,9'-spirobi[fluorene] (2.37 g, 6 mmol),PPIB (2.47 g, 5 mmol), $Pd(PPh_3)_4$ (0.17 g, 0.15 mmol), K_2CO_3 (5.52 g, 40 mmol), 20 mL distilled water, 40 mL toluene and were added to a 100 mL round flask and refluxed at 90 °C for 24 hours under nitrogen protection. Then the mixture was poured into water and extracted with dichloromethane for three times. After being collected and concentrated, the organic phase was then purified by column chromatography using petroleum ether/dichloromethane as eluent to finally afford white solid. ^{1}H NMR (500 MHz, DMSO-D_6) δ (ppm): 8.96 (d, J = 8.1 Hz, 1H), 8.90 (d, J = 8.2 Hz, 1H), 8.74 (d, J = 8.0 Hz, 1H), 8.41 (s, 1H), 8.17 (d, J = 7.6 Hz, 2H), 8.04 (d, J = 7.7 Hz, 2H), 7.75 (ddd, J = 31.0, 15.7, 7.5 Hz, 7H), 7.62 - 7.55 (m, 2H), 7.51 - 7.39 (m, 4H), 7.39 - 7.33 (m, 2H), 7.17 (dd, J = 14.2, 6.7 Hz, 3H), 7.10 (d, J = 7.8 Hz, 2H), 6.71 - 6.61 (m, 4H). MS (MALDI-TOF), m/z: calcd for $C_{52}H_{32}N_2$, 684.26; Found, 684.84 [M+]. Anal. Calcd for $C_{52}H_{32}N_2$, C,91.20; H, 4.71; N, 4.09 %; Found, C, 91.19, H, 4.73, N, 4.08%.

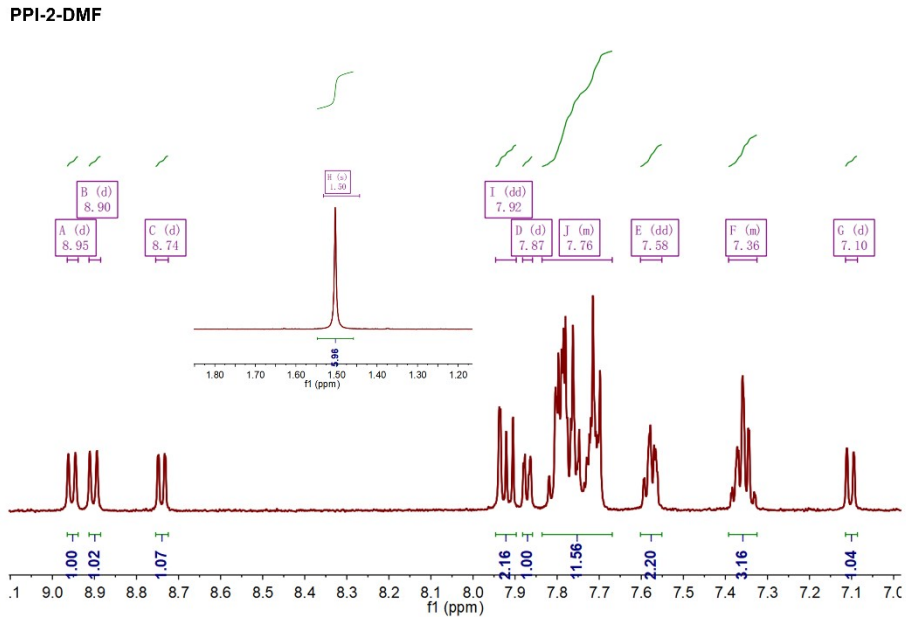

Fig S1. ^{1}H NMR spectrums of PPI-2-DMF measured in deuterated DMSO-D_6.

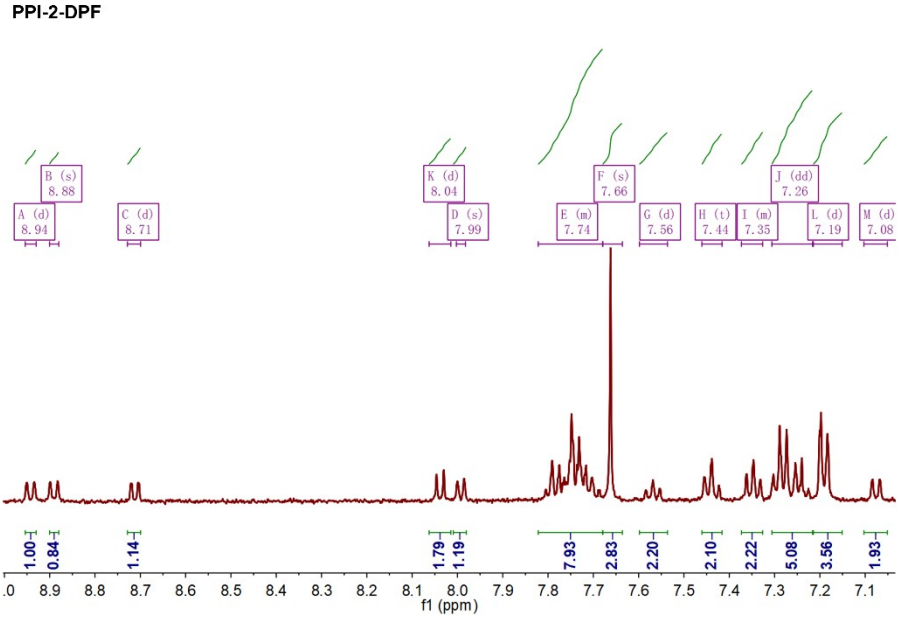

Fig S2. ^{1}H NMR spectrums of PPI-2-DPF measured in deuterated DMSO-D_6.

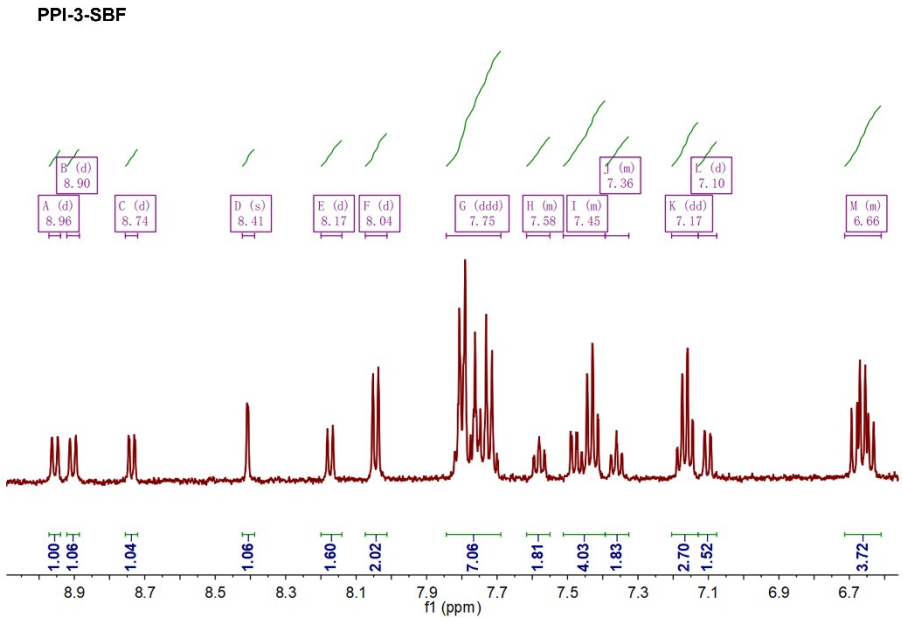

Fig S3. ^{1}H NMR spectrums of PPI-3-SBF measured in deuterated DMSO-D_6.

3. Single crystal X-ray diffraction

Table S1. Structural data of PPI-2-DMF, PPI-2-DPF and PPI-3-SBF.

compound	PPI-2-DMF	PPI-2-DPF	PPI-3-SBF
CCDC number	2167068	2167071	2167072
empirical formula	$C_{42}H_{30}N_2$	$C_{52}H_{34}N_2$	$C_{52}H_{32}N_2$
formula weight	562.68	686.81	684.79
T [K]	293	100	100
crystal system	triclinic	monoclinic	monoclinic
space group	P-1	P21/c	P21/n
a [Å]	8.635 (4)	10.3788 (3)	12.9124 (5)
b [Å]	9.812 (4)	10.8825 (4)	9.4122 (3)
c [Å]	35.662 (15)	32.3122 (12)	29.9390 (11)
α [°]	91.797 (15)	90	90
β [°]	93.504 (17)	92.934 (1)	93.272 (1)
γ [°]	90.533 (15)	90	90
V [Å^3]	3014 (2)	3644.8 (2)	3632.7 (2)

Z	4	4	4
F(000)	1184	1440	1432
density [g/cm^3]	1.240	1.252	1.252
μ [mm^{-1}]	0.072	0.072	0.072
Reflections collected	13804	8367	8338
unique reflections	7704	6027	1.059
GOF	1.033	1.052	0.1015
R_1 [I>2σ(I)]	0.0498	0.0541	0.0768
ωR_2 [I>2σ(I)]	0.1141	0.1262	0.1280
R_1 (all data)	0.1154	0.0813	1.059
ωR_2 (all data)	0.1514	0.1454	0.0441

4. Theoretical calculations

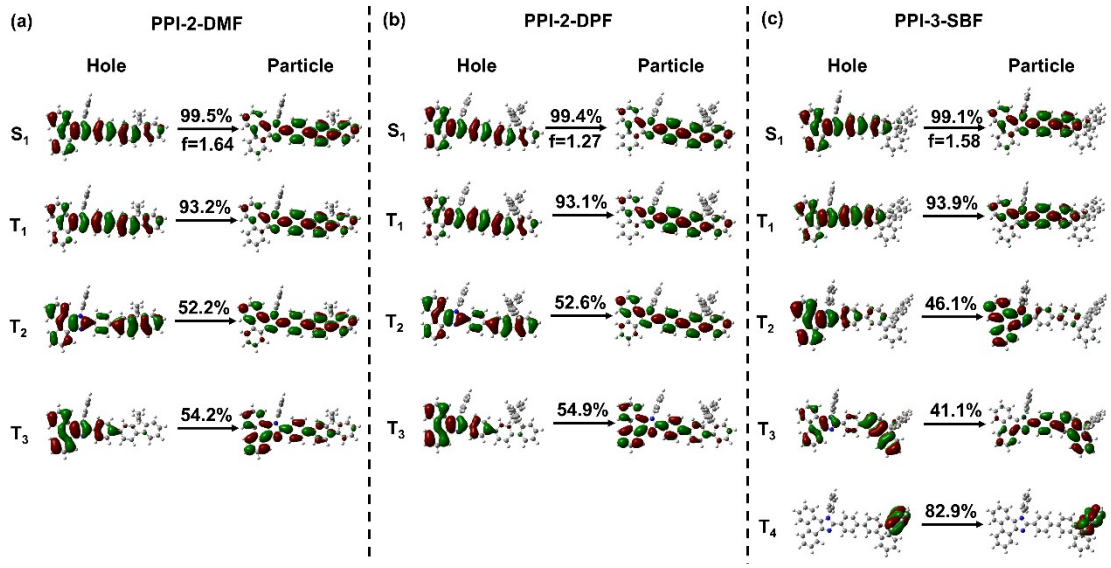

Fig S4. NTO for S_1/S_0 transition in PPI-2-DMF, PPI-2-DPF and PPI-3-SBF. Herein, f represents for the oscillator strength, and the percentage weights of hole-particle are given for the S_1/S_0 emission.

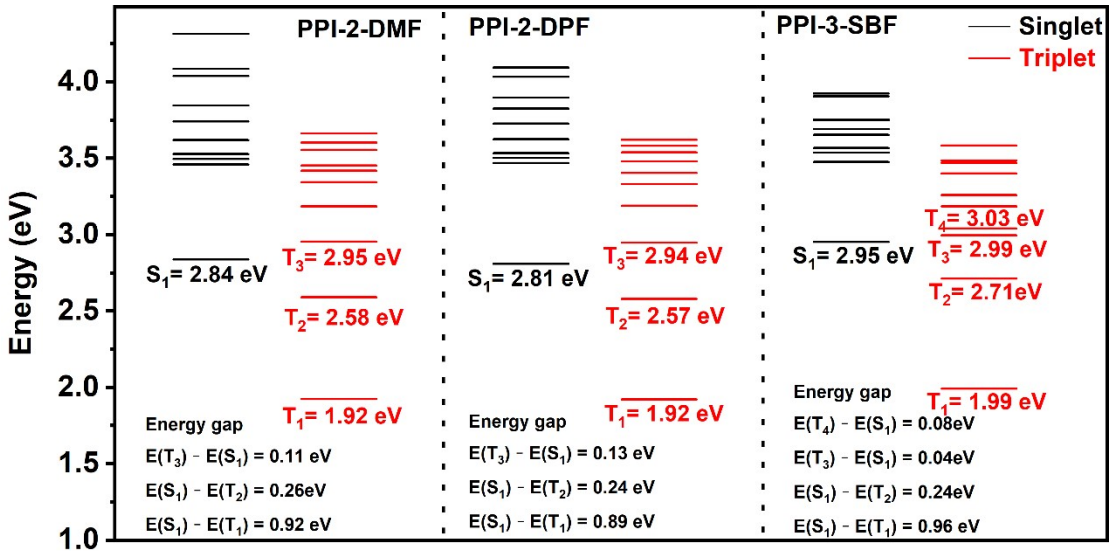

Fig S5. The energy diagram of the first ten singlet and triplet excited states of PPI-2-DMF, PPI-2-DPF and PPI-3-SBF.

5. Photophysical Properties

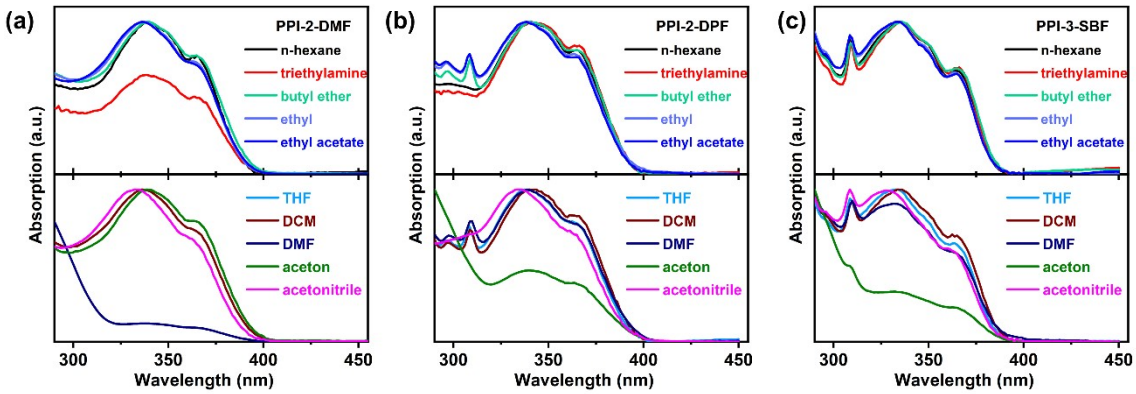

Fig S6. Solvation effects on absorption spectra of (a) PPI-2-DMF, (b) PPI-2-DPF and (c) PPI-3-SBF.

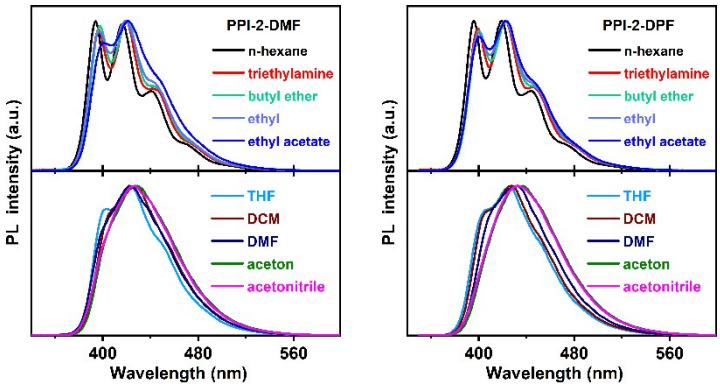

Fig S7. Solvation effects on emission spectra of PPI-2-DMF and PPI-2-DPF .

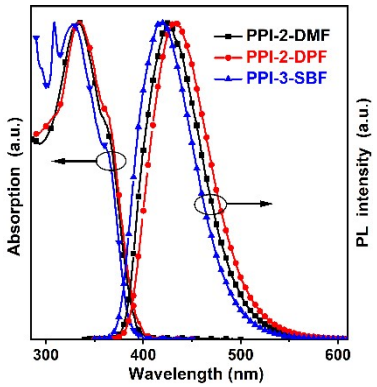

Fig S8. Absorption and PL spectra of the PPI-2-DMF, PPI-2-DPF and PPI-3-SBF in acetonitrile solution (10^{-5} M).

Table S2. Detailed photophysical data of PPI-2-DMF in different solvents.

Solvents	f (ε, n)	Φ_F	PPI-2-DMF		
			λ_{abs} (nm)	λ_{em} (nm)	ν_a-ν_f (cm^{-1})
Hexane	~ 0	86	339	393	4053
Triethylamine	0.048	46	339	396	4245
Butyl ether	0.096	66	338	397	4396
Ethyl ether	0.167	74	338	421	5719
Ethyl acetate	0.200	77	337	422	5807
Tetrahydrofuran	0.210	70	337	425	5864
Methylene chloride	0.217	77	336	426	6287
Dimethyl formamide	0.276	65	335	430	6210
Acetone	0.284	39	334	433	6465
Acetonitrile	0.305	84	332	433	6591

f: the orientational polarizability of the solvent; λ_a: absorption maximum; λ_f: emission maximum; υ_a-υ_f : the Stokes shifts.

Table S3. Detailed photophysical data of PPI-2-DPF in different solvents.

Solvents	f (ε, n)	Φ_F	PPI-2-DPF		
			λ_{abs} (nm)	λ_{em} (nm)	ν_a-ν_f (cm^{-1})
Hexane	~ 0	74	339	395	4182
Triethylamine	0.048	37	339	395	4182
Butyl ether	0.096	78	339	400	4498
Ethyl ether	0.167	83	338	407	5015
Ethyl acetate	0.200	83	338	410	5195
Tetrahydrofuran	0.210	76	337	413	5460
Methylene chloride	0.217	77	337	418	5750
Dimethyl formamide	0.276	78	336	421	6008
Acetone	0.284	45	334	417	5959
Acetonitrile	0.305	80	332	422	6423

f: the orientational polarizability of the solvent; λ_a: absorption maximum; λ_f: emission maximum; υ_a-υ_f : the Stokes shifts.

Solvents	f (ε, n)	Φ_F	PPI-3-SBF		
			λ_{abs} (nm)	λ_{em} (nm)	ν_a-ν_f (cm^{-1})
Hexane	~ 0	77	336	385	3787
Triethylamine	0.048	46	335	387	4010
Butyl ether	0.096	80	334	388	4166
Ethyl ether	0.167	88	333	409	5580
Ethyl acetate	0.200	72	333	410	5639
Tetrahydrofuran	0.210	73	333	411	5699
Methylene chloride	0.217	71	331	413	5998
Dimethyl formamide	0.276	79	330	418	6379
Acetone	0.284	43	328	418	6564
Acetonitrile	0.305	77	328	419	6621

Table S4. Detailed photophysical data of PPI-3-SBF in different solvents.
f: the orientational polarizability of the solvent; λ_a: absorption maximum; λ_f: emission maximum; υ_a-υ_f : the Stokes shifts.

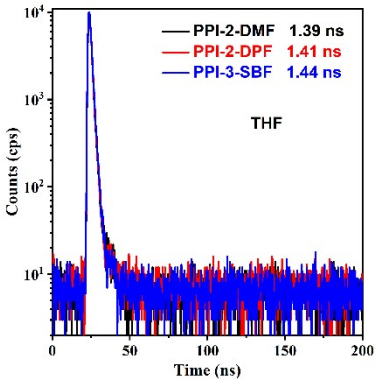

Fig S9. Transient PL decay spectra of PPI-2-DMF, PPI-2-DPF and PPI-3-SBF in THF solutions (10^{-5} M).

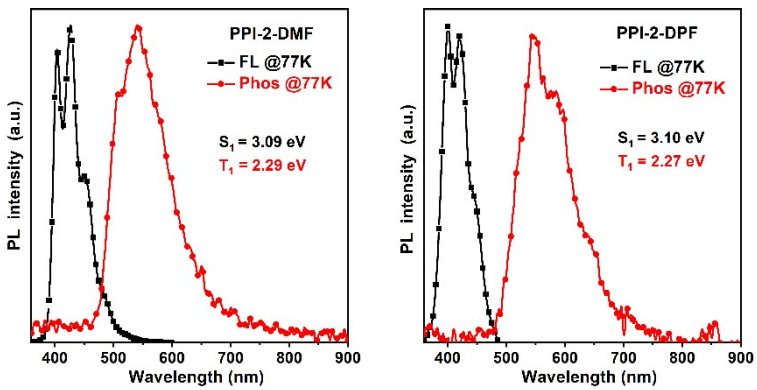

Fig S10. Low-temperature fluorescence and phosphorescence spectra at 77K of PPI-2-DMF and

PPI-2-DPF were measured in frozen toluene matrix.

6. Electrochemical properties

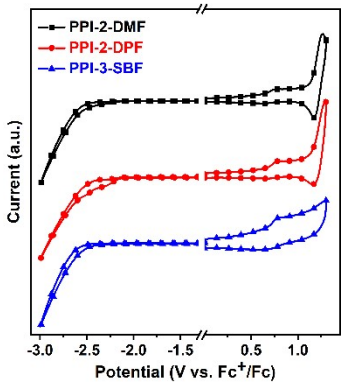

Fig S11. Cyclic voltammograms (CV) curves of PPI-2-DMF, PPI-2-DPF and PPI-3-SBF.

7. Electroluminescent properties

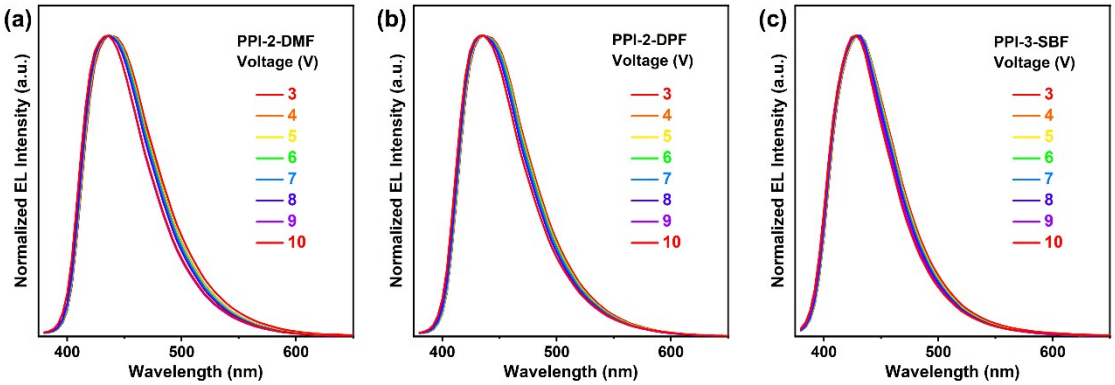

Fig S12. Normalized EL spectra of (a) PPI-2-DMF, (b) PPI-2-DPF and (c) PPI-3-SBF at different voltages.

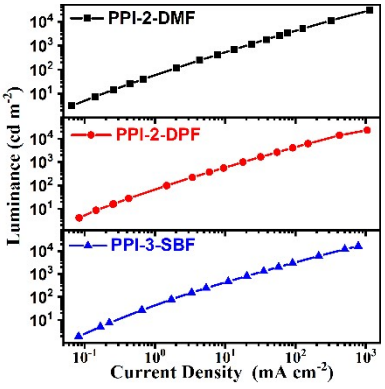

Fig S13. Current density-luminance curves of devices based on PPI-2-DMF, PPI-2-DPF and PPI-3-SBF

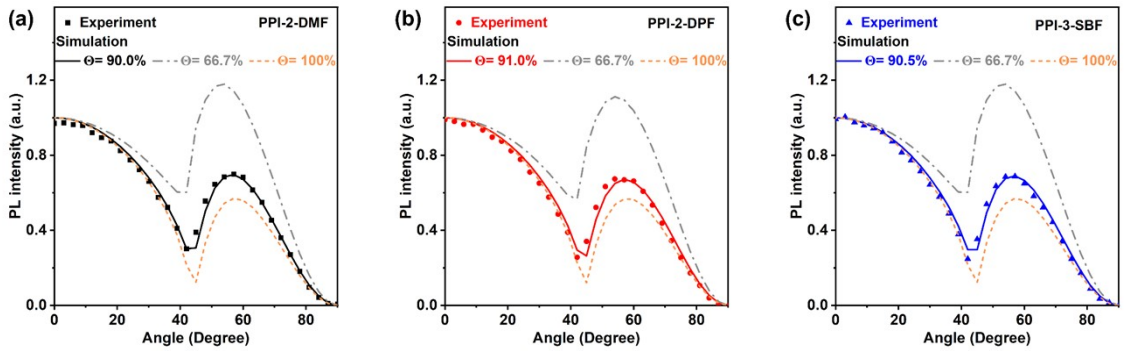

Fig S14. P-polarized PL spectra and estimated $\Theta_{//}$ values of (a) PPI-2-DMF, (b) PPI-2-DPF and (c) PPI-3-SBF neat films.

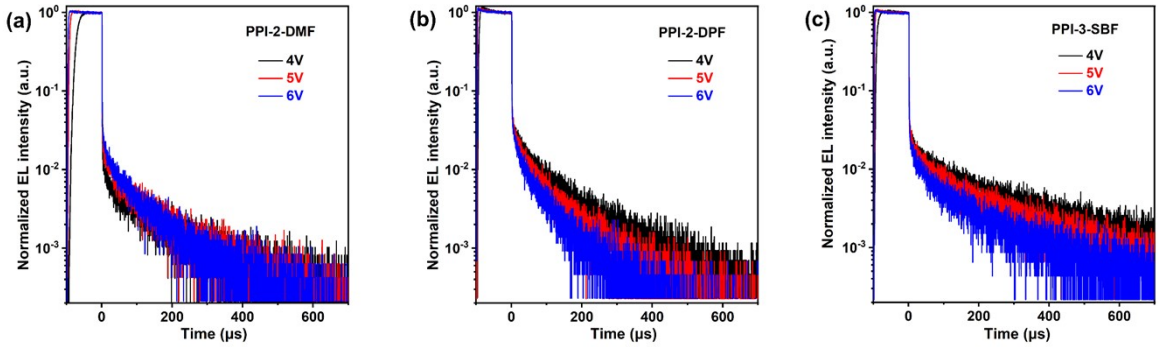

Fig S15.Transient EL decay of (a) PPI-2-DMF, (b) PPI-2-DPF and (c) PPI-3-SBF non-doped device at different voltages.

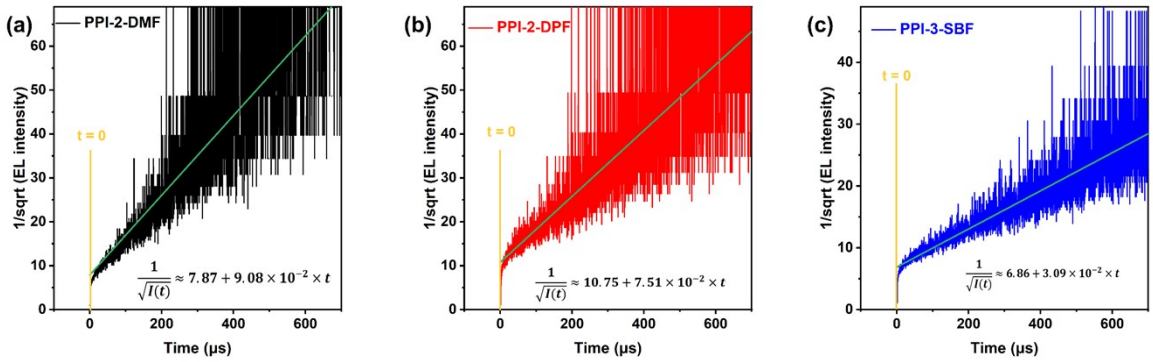

Fig S16. Inverse square root of transient EL intensity as a function of linear-scaled time.

Table S5. Recent representative high-efficiency non-doped deep blue fluorescent OLEDs with $CIE_y \leq 0.08$.

device	V_{on}[a] (V)	L_{max}[b] (cd m^{-2})	CE_{max}[c] (cd A^{-1})	PE_{max}[d] (lm W^{-1})	EQE[e] (%) Max/1000	λ_{EL}/FWHM[f] (nm)	CIE[g] (x, y)	Ref.
PPI-2-DMF	2.9	30145	5.94	5.78	7.57/6.37	434/70	(0.16, 0.09)	This work

PPI-2-DPF	2.9	23170	6.77	6.24	8.48/7.02	434/68	(0.16, 0.09)	This work
PPI-3-SBF	3.0	16365	4.72	3.69	8.41/6.77	428/60	(0.16, 0.07)	This work
2BuCz-CNCz (N)	3.6	2625	1.67	1.45	5.24/4.81	408/62	(0.157,0.050)	1
POPCN-2CP (N)	3.5	4290	--	--	7.5/6.1	404/52	(0.159, 0.035)	2
2Na-CzCN (N)	3.7	4759	1.83	1.12	5.92/5.91	398/53	(0.15, 0.06)	3
mTPA-PPI (N)	3.2	4065	0.84	0.48	3.33/--	404/47	(0.161, 0.049)	4
4-PPI-SBF	2.75	8951	2.30	2.02	5.29/--	424/--	(0.155, 0.058)	5
CSiTPI (N)	3.2	2445	1.39	1.38	7.1/--	404/45	(0.16, 0.06)	6
TPINCz (N)	3.1	--	5.00	5.15	5.95/--	448/--	(0.157, 0.084)	7
IPD-MP-DPA (N)	2.9	4158	2.4	2.5	4.4/--	428/56	(0.154,0.078)	8
2M-ph-pCzAnBzt (N)	3.4	3085	5.95	5.43	10.44/--	450/--	(0.151, 0.057)	9
TPA-PI-SBF (N)	3.1	4901	3.61	3.50	6.76/6.71	448/59	(0.152, 0.059)	10
TPBPPI-PBI (N)	3.9	--	3.22	2.71	5.94/--	429/--	(0.160, 0.059)	11
PIpPI (N)	3.0	17560	5.33	5.31	8.84/7.70	428/--	(0.15, 0.07)	12
2FPPITPA (N)	2.8	3798	6.47	7.00	8.47/6.90	440/--	(0.152, 0.083)	13
PPI-2TPA (N)	3.0	14850	4.40	4.60	7.20/--	440/59	(0.150, 0.063)	14
9-PCZCFOXZ(N)	3.2	5740	4.1	2.9	7.2/5.0	417/--	(0.153, 0.075)	15
SP (N)	3.0	13488	6.9	7.5	11.3/7.0	436/--	(0.158, 0.068)	16

[a]$V_{on:}$ turn-on voltage at the luminescence of 1 cd m^{-2}; [b]$L_{max:}$ maximum luminance; [c]$CE_{max:}$ maximum current efficiency; [d]$PE_{max:}$ maximum power efficiency; [e]EQE max/1000: EQE of maximum /1000 cd m^{-2}; [f]λ_{EL}/FWHM: emission peak and full widths at half maximum of EL spectrum; [g]CIE: Commission International de l'Éclairage (CIE) coordinates.

References:

1. H. Zhang, G. Li, X. Guo, K. Zhang, B. Zhang, X. Guo, Y. Li, J. Fan, Z. Wang, D. Ma and B. Z. Tang, Angew. Chem. Int. Ed., 2021, 60, 22241-22247.

2. J. Chen, H. Liu, J. Guo, J. Wang, N. Qiu, S. Xiao, J. Chi, D. Yang, D. Ma, Z. Zhao and B. Z. Tang, Angew. Chem. Int. Ed., 2022, 61, e202116810.

3. G. Li, B. Li, H. Zhang, X. Guo, C. Lin, K. Chen, Z. Wang, D. Ma and B. Z. Tang, ACS Appl. Mater. Interfaces, 2022, 14, 10627-10636.

4. H. Liu, Q. Bai, L. Yao, H. Zhang, H. Xu, S. Zhang, W. Li, Y. Gao, J. Li, P. Lu, H. Wang, B. Yang and Y. Ma, Chem. Sci., 2015, 6, 3797-3804.

5. Z.-Y. Wang, J.-W. Zhao, B. Liu, C. Cao, P. Li, Q.-X. Tong and S.-L. Tao, Dyes Pigm., 2019, 163, 213-220.

6. Y. Zheng, X. Zhu, Z. Ni, X. Wang, Z. Zhong, X. J. Feng, Z. Zhao and H. Lu, Adv. Opt. Mater., 2021, 9, 2100965.

7. W.-C. Chen, Y. Yuan, S.-F. Ni, Q.-X. Tong, F.-L. Wong and C.-S. Lee, Chem. Sci., 2017, 8, 3599-3608.

8. J. Xu, H. Liu, J. Li, Z. Zhao and B. Z. Tang, Adv. Opt. Mater., 2021, 9, 2001840.

9. R. Guo, W. Liu, S. Ying, Y. Xu, Y. Wen, Y. Wang, D. Hu, X. Qiao, B. Yang, D. Ma and L. Wang, Sci. Bull., 2021, 66, 2090-2098.

10. S.-S. Tang, G.-X. Yang, J.-J. Zhu, X. He, J.-X. Jian, F. Lu and Q.-X. Tong, Chem. Eur. J., 2021, 27, 9102-9111.

11. J.-J. Zhu, W.-C. Chen, Y. Yuan, D. Luo, Z.-L. Zhu, X. Chen, J.-X. Chen, C.-S. Lee and Q.-X. Tong, Dyes Pigm., 2020, 173, 107982.

12. Z. Li, C. Li, Y. Xu, N. Xie, X. Jiao and Y. Wang, J. Phys. Chem. Lett., 2019, 10, 842-847.

13. Z. Li, N. Xie, Y. Xu, C. Li, X. Mu and Y. Wang, Org. Mater., 2020, 02, 011-019.

14. B. Liu, Z.-W. Yu, D. He, Z.-L. Zhu, J. Zheng, Y.-D. Yu, W.-F. Xie, Q.-X. Tong and C.-S. Lee, J. Mater. Chem. C, 2017, 5, 5402-5410.

15. R. Wang, T. Li, C. Liu, M. Xie, H. Zhou, Q. Sun, B. Yang, S.-T. Zhang, S. Xue and W. Yang, Adv. Funct. Mater., 2022, 32, 2201143.

16. S. Xiao, Y. Gao, R. Wang, H. Liu, W. Li, C. Zhou, S. Xue, S.-T. Zhang, B. Yang and Y. Ma, Chem. Eng. J. , 2022, 440, 135911.